crystals

MDPI

Article

Synthesis, Characterization and DFT Calculation of Naphthalene-Based Crystal Structure with Pyridylimine-Binding Units

Babak Mirtamizdoust [1], Amirhossein Karamad [1], Negin Rahmani [2], Younes Hanifehpour [2,*] and Sang Woo Joo [3,*]

[1] Department of Chemistry, Faculty of Science, University of Qom, Qom 37185359, Iran; babak.mirtamizdoust@qom.ac.ir (B.M.); karamad1995@gmail.com (A.K.)
[2] Department of Chemistry, Faculty of Science, Sayyed Jamaleddin Asadabadi University, Asadabad 6541861841, Iran; rahmani.negin2004@gmail.com
[3] School of Mechanical Engineering, Yeungnam University, Gyeongsan 712-749, Republic of Korea
* Correspondence: younes.hanifehpour@gmail.com (Y.H.); swjoo@yu.ac.kr (S.W.J.)

Abstract: This study focuses on the synthesis, characterization, and properties of a yellowish, prism-shaped ligand, N,N′-(naphthalene-1,5-diyl) bis(1-(pyridin-2-yl) methanimine). The ligand was synthesized through refluxing 1,5-diaminonaphthalene and pyridine-2-carbaldehyde in extra-pure ethanol, employing X-ray diffraction on single crystal. The crystal is structured with two pyridylimine-binding units linked to a naphthalene. The crystal has a $P2_1/c$ space group in a monoclinic system. The structure was confirmed through an infrared examination. Computational spectroscopy and theoretical methods were used to investigate the ligand HOMO, LUMO, and charge distribution. Additionally, a Hirshfeld analysis was performed to investigate noncovalent interactions in the crystalline form. The results showed that dispersion forces (H···H) were the primary factor contributing to the arrangement of the ligand molecule, accounting for 45.3% of the total interactions in the absence of hydrogen bonding. Overall, this study provides valuable insights into the synthesis, characterization, and properties of this unique ligand.

Keywords: Schiff-base; aromatic; weak interaction; crystal structure

Citation: Mirtamizdoust, B.; Karamad, A.; Rahmani, N.; Hanifehpour, Y.; Joo, S.W. Synthesis, Characterization and DFT Calculation of Naphthalene-Based Crystal Structure with Pyridylimine-Binding Units. *Crystals* **2023**, *13*, 1129. https://doi.org/10.3390/cryst13071129

Academic Editor: Vladimir P. Fedin

Received: 20 June 2023
Revised: 9 July 2023
Accepted: 18 July 2023
Published: 19 July 2023

1. Introduction

Various fields benefit from a diverse array of practical implementations of structures based on naphthalene [1,2]. Imine systems can also be utilized to assemble discrete cyclophanes, double and triple helicates, dimers, trimmers, and grids [3–13]. One of the factors, which could affect these structure properties can be short contact. The formation of three-dimensional structures in biological and chemical systems relies heavily on short-range interactions, which can also aid in the creation of new materials with beneficial properties [14–17]. The other importance of short contacts is that these contacts a considerable impact on the physical and chemical properties of a compound, including its melting point, boiling point, and reactivity [18]. The study of short contacts in organic structures has gained increasing attention in recent years. This interest has been driven by advances in computational chemistry, which have made it possible to study the properties and behavior of organic compounds at the molecular level. Here we synthesized and characterized a structure that has two parallel pyridylimine binding units on both sides. These kinds of structures, which look rigid, can support grid structures such as Oborn and Youinou [19] or Lehn [20]. A similar structure on both sides of naphthalene has been observed in the works of other researchers, such as Piontek [21]. In this article, we will explore the synthesis, characterization, and DFT calculation of naphthalene-based crystal structures with pyridylimine-binding units.

2. Experimental

2.1. Synthesis

The ligand was made by refluxing 1,5-diaminonaphthalene (1 mol, 158.20 g) and pyridine-2-carbaldehyde (2 mol, 214.22 g) for 10 h in extra-pure ethanol. The crystal was washed with an ethanol/acetone solution and dried at 60 °C. Analysis calculated for $C_{22}H_{16}N_4$: C, 78.55; H, 4.79; N, 16.66. Found: C, 79.00; H, 5.00; N, 16.00. Characteristic FT-IR data (KBr, cm^{-1}): 519, 628, 996, 1063, 1108, 1448, 1359, 1592, 3261, 3421. Scheme 1 demonstrates the ligand preparation.

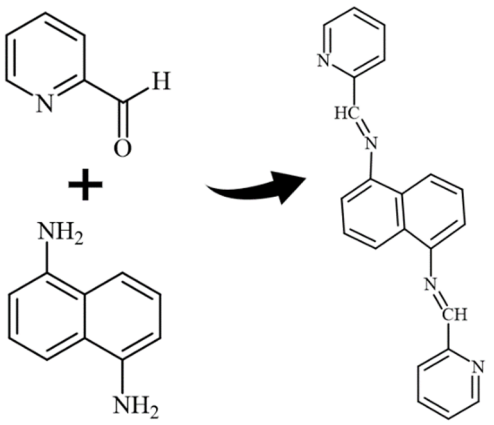

Scheme 1. Ligand preparation.

2.2. X-ray Diffraction

The compound formed a yellowish, prism-shaped crystal measuring 0.06 × 0.06 × 0.30 mm^3. The crystal was placed on a glass fiber and cooled to −93 °C using a nitrogen gas stream controlled by the Cryostream Controller 700. X-ray diffraction data were collected using a Bruker SMART APEX II instrument (Madison, WI, USA). The instrument used graphite-monochromated Mo Kα radiation (λ = 0.71073 Å). The diffractometer operated at 50 kV and 30 mA. The data was collected over 2θ ranges of 8.08~52.00°. The data collection process did not show any significant decay.

The data processing steps were performed on a PC using the Bruker AXS Crystal Structure Analysis Package [22–25]: The following steps were taken: The data were collected using APEX2, and cell refinement and data reduction were performed with SAINT. Absorption correction was carried out using SADABS, while the structure solution involved the use of XPREP and SHELXS-97. Structure refinement was performed with SHELXL-97, and molecular graphics and publication materials were generated using SHELXTL [26]. Cromer and Waber were the sources of the neutral atom scattering factors [27]. The monoclinic space group $P2_1/c$ was identified through E statistics, systematic absences, and successful structure refinement. Direct methods were used to solve the structure. The compound was refined using full-matrix least-squares, with a minimization function of $\sum w\ (Fo^2 - Fc^2)^2$. All non-hydrogen atoms underwent anisotropic refinement. Hydrogen atoms were positioned geometrically with a C-H distance of 0.95 Å and refined as riding atoms with a Ui-so(H) value of 1.2 UeqC. For 1204 independent reflections with I > 2σ(I), the final R_1 value was 0.0410 and wR_2 was 0.0872. For all 1599 independent reflections with R(int) = 0.0250, the final R_1 value was 0.0606 and wR_2 was 0.1021. The refinement involved 118 parameters and 0 restraints ($R_1 = \sum||Fo| - |Fc||/\sum|Fo|$; $wR_2 = \{\sum[w\ (Fo^2 - Fc^2)^2]/\sum[w(Fo^2)^2]\}^{1/2}$; $(w = 1/[\sigma^2(Fo^2) + (0.0364P)^2 + 0.2981P]$, where $P = [Max\ (Fo^2, 0) + 2Fc^2]/3)$). The largest residual peak was 0.200 e/$Å^3$, and the largest residual hole was −0.231 e/$Å^3$. The crystallographic data for compound **1** has been deposited with the Cambridge Crystallographic Data Centre as Supplementary Publication CCDC-2252233. The crystal characteristics and structure refinement were presented in Table 1. Tables 2–6 provide additional crystallographic information, including atomic

coordinates (Table 2), bond lengths (Table 3), angles (Table 3), anisotropic displacement parameters (Table 4), hydrogen coordinates (Table 5), and torsion angles (Table 6).

Table 1. Crystal data and structure refinement.

Formula	C_{22} H_{16} N_4	
Formula weight	336.39	
Temperature	180 (2) K	
Wavelength	0.71073 Å	
Crystal system	Monoclinic	
Space group	$P2_1/c$	
Unit cell dimensions	a = 4.8908 (2) Å	α = 90°
	b = 16.8343 (7) Å	β = 91.106 (2)°
	c = 10.0884 (4) Å	γ = 90°
Volume	830.46 (6) $Å^3$	
Z	2	
Density	1.345 Mg/m^3	
Absorption coefficient	0.082 mm^{-1}	
F(000)	352	
Crystal size	0.20 × 0.06 × 0.06 mm^3	
Theta range for data collection	4.04 to 25.98°	
Index ranges	$-6 \leq h \leq 5$, $-20 \leq k \leq 12$, $-12 \leq l \leq 9$	
Reflections collected	2869	
Independent reflections	1599 [R (int) = 0.0250]	
Completeness to theta= 25.98°	98.80%	
Absorption correction	Multi-scan	
Maximum and minimum transmission	0.9951, 0.9837	
Refinement method	Full-matrix least-squares on F^2	
Data/restraints/parameters	1599/0/118	
Goodness–of-fit on F^2	1.034	
Final R indices [I > 2sigma(I)]	R_1 =0.0410, wR_2= 0.0872	
R indices (all data)	R_1 =0.0606, wR_2= 0.1021	
Largest diff. peak and hole	0.200 and −0.231 e/$Å^3$	

Table 2. The atomic coordinates are expressed in units of 10^{-4}, while the equivalent isotropic displacement parameters are expressed in units of 10^{-3} $Å^2$. U (eq) is defined as one-third of the trace of the orthogonalized Uij tensor.

	x	y	z	U (eq)
N (1)	−1614 (3)	3811 (1)	4851 (1)	35 (1)
N (2)	2688 (3)	3992 (1)	7709 (1)	28 (1)
C (1)	−3381 (4)	3309 (1)	4265 (2)	38 (1)
C (2)	−3915 (4)	2552 (1)	4706 (2)	35 (1)
C (3)	−2561 (4)	2291 (1)	5832 (2)	35 (1)
C (4)	−731 (4)	2793 (1)	6466 (2)	33 (1)
C (5)	−301 (3)	3546 (1)	5951 (2)	27 (1)
C (6)	1518 (3)	4131 (1)	6597 (2)	27 (1)
C (7)	4348 (3)	4594 (1)	8288 (2)	25 (1)
C (8)	6167 (3)	5039 (1)	7575 (2)	28 (1)
C (9)	7851 (3)	5604 (1)	8210 (2)	29 (1)
C (10)	7705 (3)	5729 (1)	9543 (2)	27 (1)
C (11)	4154 (3)	4709 (1)	9688 (2)	23 (1)

It might be interesting to present crystallography data in a visual format to provide a clear understanding of these pieces of information. Thus, we provided some Figure 1.

Table 3. Bond lengths [Å] and angles [°].(Symmetry transformations used to generate equivalent atoms: #1 − x + 1, −y + 1, −z + 2).

Length [Å]		Angle [°]			
N (1)-C (1)	1.338 (2)	C (1)-N (1)-C (5)	116.67 (15)	C (7)-C (8)-H (8A)	119.7
N (1)-C (5)	1.348 (2)	C (6)-N (2)-C (7)	118.43 (14)	C (9)-C (8)-H (8A)	119.7
N (2)-C (6)	1.272 (2)	N (1)-C (1)-C (2)	124.50 (17)	C (10)-C (9)-C (8)	120.83 (16)
N (2)-C (7)	1.418 (2)	N (1)-C (1)-H (1A)	117.7	C (10)-C (9)-H (9A)	119.6
C (1)-C (2)	1.377 (3)	C (2)-C (1)-H (1A)	117.7	C (8)-C (9)-H (9A)	119.6
C (1)-H (1A)	0.95	C (3)-C (2)-C (1)	118.13 (17)	C (9)-C (10)-C (11) #1	120.43 (16)
C (2)-C (3)	1.376 (2)	C (3)-C (2)-H (2A)	120.9	C (9)-C (10)-H (10A)	119.8
C (2)-H (2A)	0.95	C (1)-C (2)-H (2A)	120.9	C (11) #1-C (10)-H (10A)	119.8
C (3)-C (4)	1.379 (2)	C (2)-C (3)-C (4)	118.99 (17)	C (10) #1-C (11)-C (11) #1	119.42 (18)
C (3)-H (3A)	0.95	C (2)-C (3)-H (3A)	120.5	C (10) #1-C (11)-C (7)	121.81 (15)
C (4)-C (5)	1.387 (2)	C (4)-C (3)-H (3A)	120.5	C (11) #1-C (11)-C (7)	118.76 (18)
C (4)-H (4A)	0.95	C (3)-C (4)-C (5)	119.22 (16)		
C (5)-C (6)	1.470 (2)	C (3)-C (4)-H (4A)	120.4		
C (6)-H (6A)	0.95	C (5)-C (4)-H (4A)	120.4		
C (7)-C (8)	1.376 (2)	N (1)-C (5)-C (4)	122.49 (16)		
C (7)-C (11)	1.430 (2)	N (1)-C (5)-C (6)	114.71 (15)		
C (8)-C (9)	1.404 (2)	C (4)-C (5)-C (6)	122.74 (15)		
C (8)-H (8A)	0.95	N (2)-C (6)-C (5)	121.71 (15)		
C (9)-C (10)	1.365 (2)	N (2)-C (6)-H (6A)	119.1		
C (9)-H (9A)	0.95	C (5)-C (6)-H (6A)	119.1		
C (10)-C (11) #1	1.414 (2)	C (8)-C (7)-N (2)	123.00 (14)		
C (10)-H (10A)	0.95	C (8)-C (7)-C (11)	119.92 (15)		
C (11)-C (10) #1	1.414 (2)	N (2)-C (7)-C (11)	117.03 (14)		
C (11)-C (11) #1	1.422 (3)	C (7)-C (8)-C (9)	120.63 (15)		

Table 4. The anisotropic displacement parameters expressed in units of $Å^2 \times 10^3$. The exponent of the anisotropic displacement factor is given by the formula: $-2\pi^2$ [$h^2a^{*2}U^{11}$ + ... + 2 h k a* b* U^{12}].

	U^{11}	U^{22}	U^{33}	U^{23}	U^{13}	U^{12}
N (1)	48 (1)	31 (1)	26 (1)	0 (1)	−8 (1)	−4 (1)
N (2)	30 (1)	26 (1)	26 (1)	−4 (1)	−3 (1)	2 (1)
C (1)	49 (1)	37 (1)	28 (1)	−2 (1)	−13 (1)	−3 (1)
C (2)	37 (1)	33 (1)	33 (1)	−7 (1)	−4 (1)	−5 (1)
C (3)	40 (1)	28 (1)	37 (1)	1 (1)	−1 (1)	−3 (1)
C (4)	37 (1)	31 (1)	30 (1)	2 (1)	−5 (1)	1 (1)
C (5)	30 (1)	29 (1)	23 (1)	−3 (1)	−1 (1)	1 (1)
C (6)	32 (1)	23 (1)	28 (1)	0 (1)	0 (1)	1 (1)
C (7)	27 (1)	21 (1)	27 (1)	−2 (1)	−5 (1)	5 (1)
C (8)	31 (1)	27 (1)	25 (1)	0 (1)	−1 (1)	5 (1)
C (9)	29 (1)	29 (1)	31 (1)	3 (1)	1 (1)	−1 (1)
C (10)	27 (1)	24 (1)	31 (1)	−1 (1)	−3 (1)	0 (1)
C (11)	23 (1)	20 (1)	26 (1)	1 (1)	−3 (1)	5 (1)

Table 5. Units of Measurement for Hydrogen Coordinates ($\times 10^4$) and Isotropic Displacement Parameters ($Å^2 \times 10^3$).

	x	y	z	U (eq)
H (1A)	−4333	3488	3491	46
H (2A)	−5184	2220	4246	41
H (3A)	−2881	1773	6167	42
H (4A)	224	2625	7246	39
H (6A)	1828	4625	6171	33
H (8A)	6285	4963	6645	33
H (9A)	9107	5903	7704	35
H (10A)	8861	6113	9958	33

Table 6. Torsion angle [°].(Symmetry transformations used to generate equivalent atoms: #1 − x + 1, −y + 1, −z + 2).

C (5)-N (1)-C (1)-C (2)	−0.4 (3)
N (1)-C (1)-C (2)-C (3)	0.5 (3)
C (1)-C (2)-C (3)-C (4)	−0.2 (3)
C (2)-C (3)-C (4)-C (5)	−0.1 (3)
C (1)-N (1)-C (5)-C (4)	0.1 (3)
C (1)-N (1)-C (5)-C (6)	−177.18 (15)
C (3)-C (4)-C (5)-N (1)	0.2 (3)
C (3)-C (4)-C (5)-C (6)	177.22 (16)
C (7)-N (2)-C (6)-C (5)	−178.12 (15)
N (1)-C (5)-C (6)-N (2)	173.21 (16)
C (4)-C (5)-C (6)-N (2)	−4.0 (3)
C (6)-N (2)-C (7)-C (8)	−43.3 (2)
C (6)-N (2)-C (7)-C (11)	139.21 (16)
N (2)-C (7)-C (8)-C (9)	−177.12 (15)
C (11)-C (7)-C (8)-C (9)	0.3 (2)
C (7)-C (8)-C (9)-C (10)	−0.5 (3)
C (8)-C (9)-C (10)-C (11) #1	−0.1 (2)
C (8)-C (7)-C (11)-C (10) #1	179.36 (15)
N (2)-C (7)-C (11)-C (10) #1	−3.1 (2)
C (8)-C (7)-C (11)-C (11) #1	0.6 (3)
N (2)-C (7)-C (11)-C (11) #1	178.14 (17)

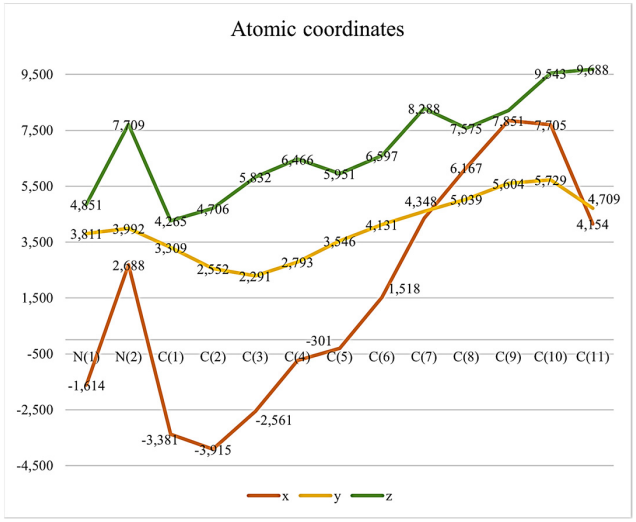

(**a**)

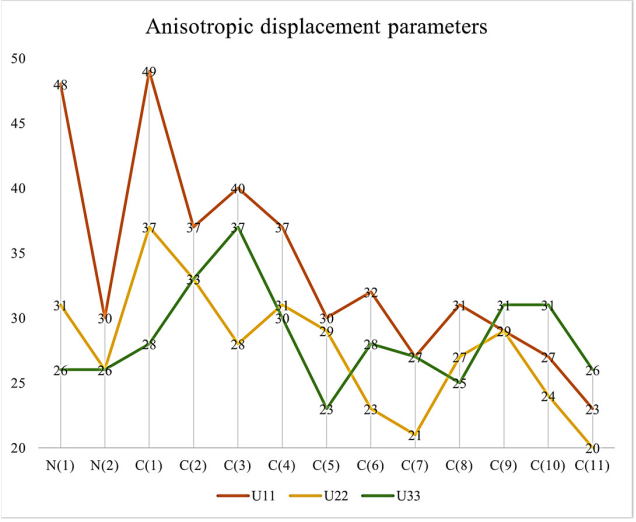

(**b**)

Figure 1. *Cont.*

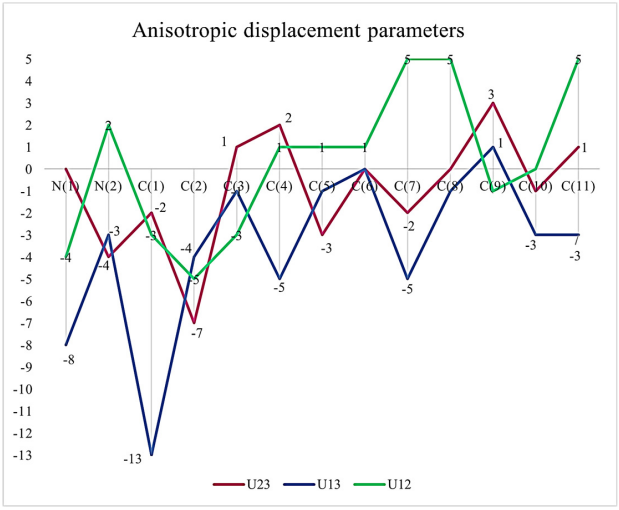

(**c**)

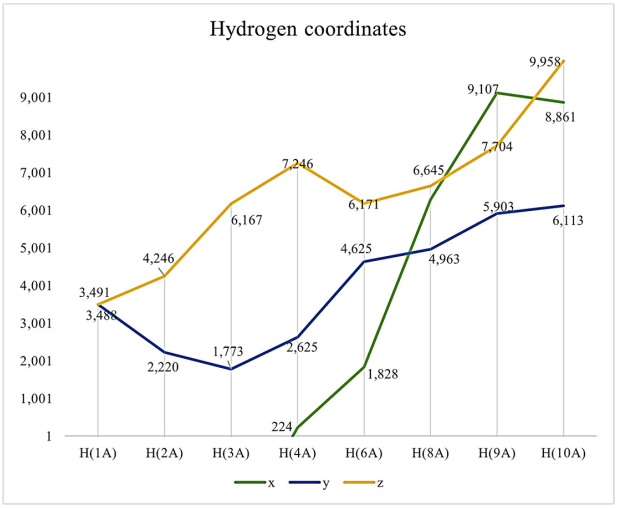

(**d**)

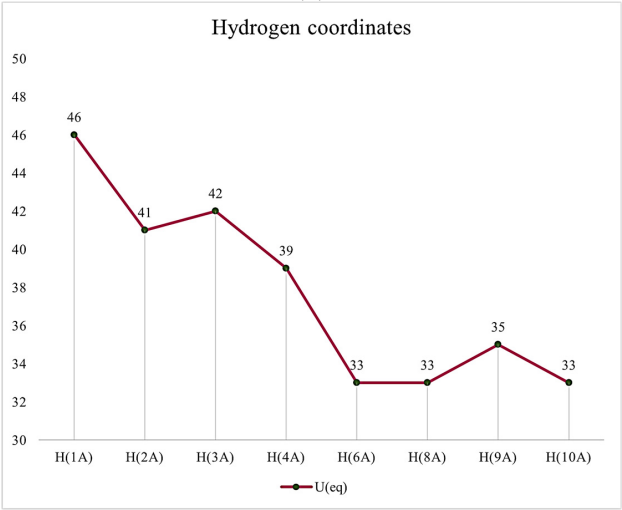

(**e**)

Figure 1. (**a**) Atomic Coordinates ($\times 10^4$). (**b**) Anisotropic displacement parameters (Å^2 $\times$ 10^3) U^{11}, U^{22}, U^{33}. (**c**) Anisotropic displacement parameters (Å^2 $\times$ 10^3) U^{23}, U^{13}, U^{12}. (**d**) Hydrogen Coordinates ($\times 10^4$). (**e**) Isotropic displacement parameters (Å^2 $\times$ 10^3).

2.3. IR Characterization

Confirmation of the successful synthesis of the ligand was obtained through analysis of the IR. The spectrum displays a strong peak at 1288 cm^{-1}, indicating the stretching frequency due to aromatic nitrogen. Additionally, there are two medium peaks at 1384 cm^{-1} and 1414 cm^{-1}, which correspond to the deformation of CH_2 and CH_3, respectively. The medium peak at 1472 cm^{-1} is attributed to the symmetric bending vibration of the CH_2 group. The weak peak at 1514 cm^{-1} in the IR spectrum is caused by the bending vibration of the aromatic ring in the compound. Figure 2 demonstrates IR spectrum.

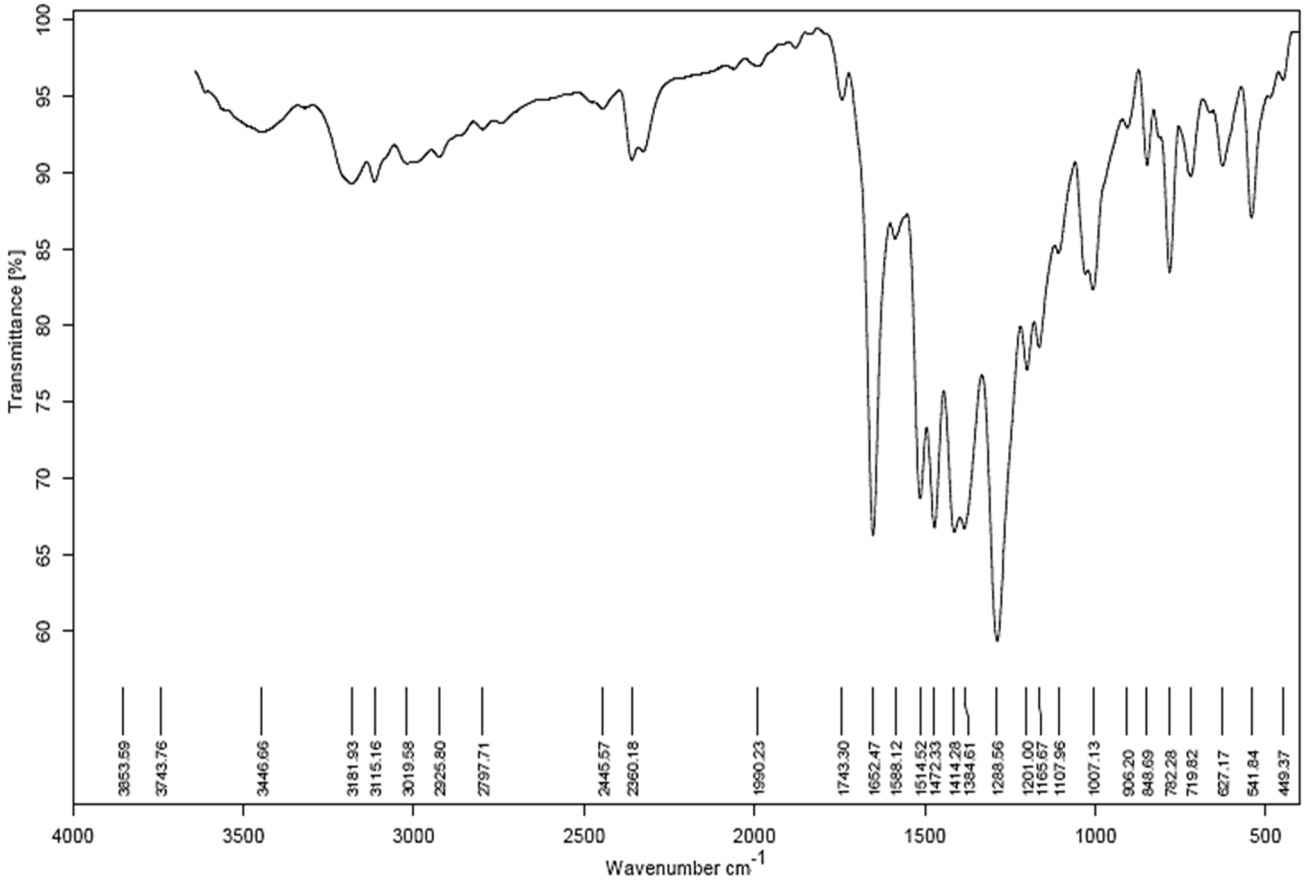

Figure 2. IR spectrum.

2.4. Computational Method

For this research, we utilized GaussView 6.0 and Gaussian 09W software on a Windows operating system. To make the Gaussian work more manageable, we broke it down into two steps and completed them separately. Initially, we optimized the structure, and subsequently, we used the output file from the previous step to compute the Raman, NMR, HUMO, and LUMO structures.

2.5. Hirshfeld Surface Analysis

To perform an analysis of intermolecular contacts in the crystals under investigation, the Crystal Explorer Ver. 3.1 program package was used [28]. This involved utilizing Hirshfeld surface analyses, 2D fingerprint plots, and calculating the percentage contributions.

3. Results and Discussion

X-ray diffraction analysis was used to determine the structure of the ligand, revealing that it has a symmetrical structure with naphthalene in the center and two pyridines on the sides and belongs to the $P2_1/c$ space group in a monoclinic system. C (7) on naphthalene

and N (2) on the sides, connected naphthalene and pyridine with bond length 1.418 (2) to form a molecule structure (Figure 3a). Figure 3b depicts the unit cell packing. The multi-layer structure shows empty spaces in the unit cell in Figure 3b. Another structure, Figure 3c, is created by the direct growth of the compound structure and bears a striking resemblance to the Z shape when viewed from a specific orientation. Figure 3: The molecular structure: (a) The molecular structure (50% probability); (b) Unit cell packing; (c) The Z shape structure.

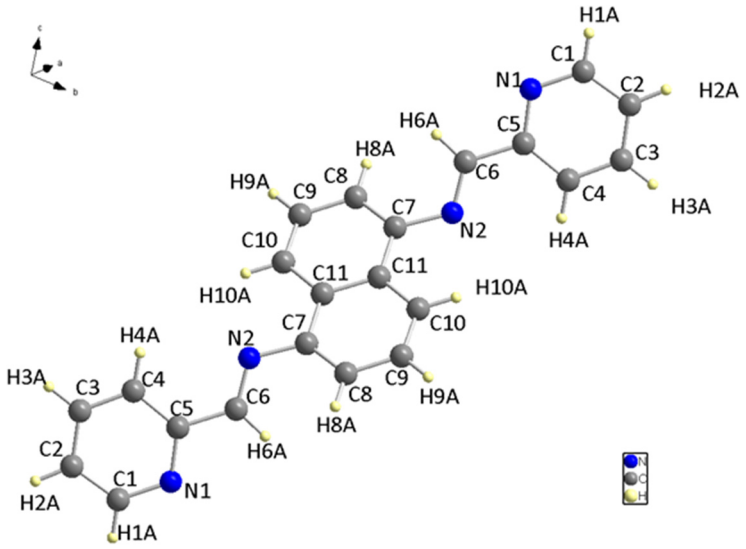

(**a**)

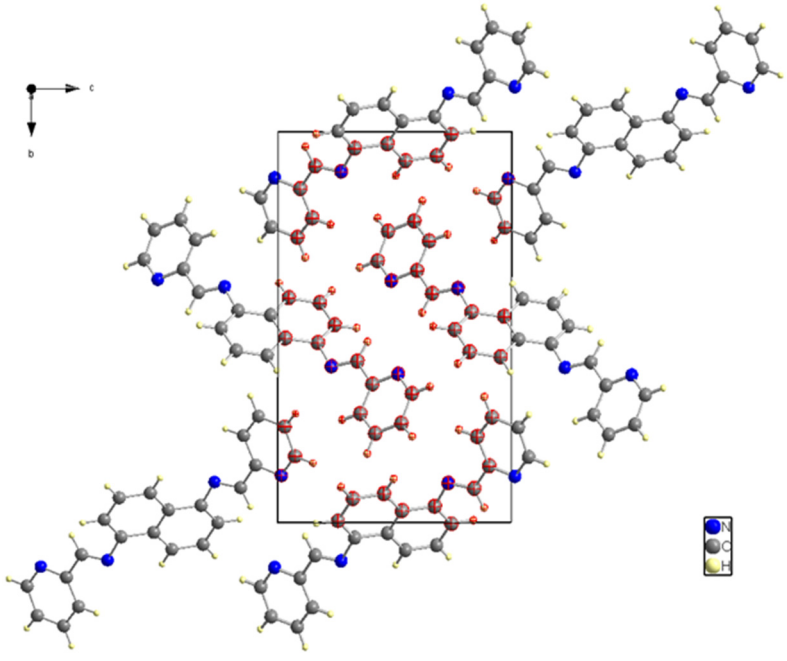

(**b**)

Figure 3. *Cont.*

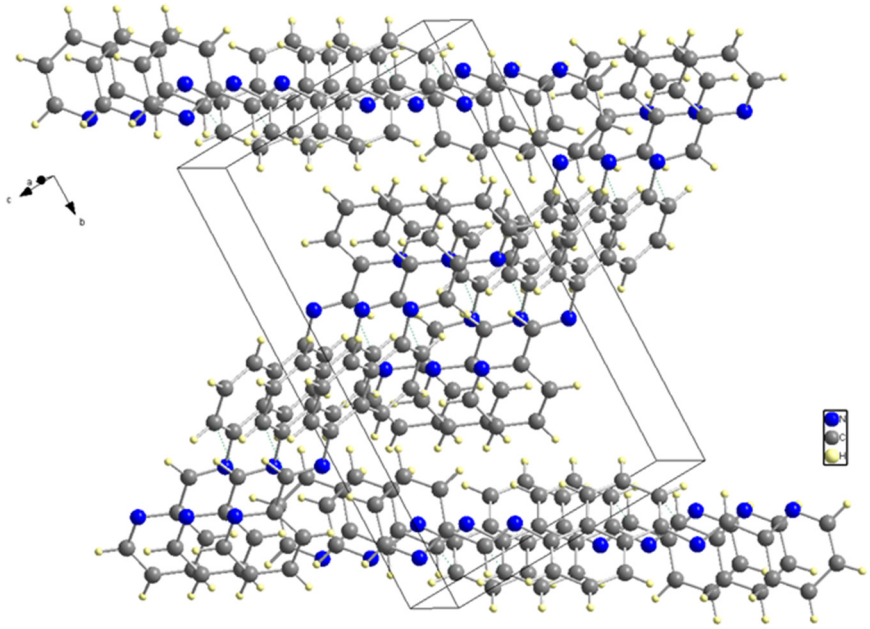

(**c**)

Figure 3. (**a**) The molecular structure. (**b**) Unit cell packing. (**c**) The Z shape structure.

The bond between C (5) and C (6) has the longest bond length at 1.470 (2) Å. N (2) is bonded to C (7) on one side and C (6) on the other, with bonding distances of 1.418 (2) Å and 1.272 (2) Å, respectively. Additionally, the bond between N (2) and C (6) on both sides is the shortest non-hydrogen ligand bond.

The nitrogen and carbon bonds mentioned have slight differences compared to other nitrogen (N (1)) and carbon bonds within the ligand. At the ligand ends, we find N (1)-C (1) and N (1)-C (5), which measure 1.338 (2) Å and 1.348 (2) Å, respectively. The title compound molecule has a linker section (C (7)-N (2)-C (6)-C (5)) with an angle of −178.12° (15). There are no hydrogen bonding interactions present in the structure. The structure shown in Figure 4 is a result of the short contacts caused by C (6) and C (8), which attract neighboring molecules.

Computational studies with Gaussian were conducted in this research, and Table 7 provides a summary of the ligand calculation obtained in the 6-311+(2d, p) basis set. The results suggest that the molecule is nonpolar or only slightly polar, which is supported by the very small dipole moment of 0.000039 D. This value indicates that there is minimal charge separation within the molecule. These findings align with previous discussions.

Table 7. Gaussian calculation summary.

Basis Set	6-311+(2d, p)	
Charge	0	
Spin	Singlet	
Solvation	None	
Electronic Energy	−1067.265351	Hartree
RMS Gradient Norm	0.000014	Hartree/Bohr
Dipole Moment	0.000039	Debye
Polarizability (α)	350.831853	a.u.
Hyperpolarizability (β)	0.016519	a.u.

The charge distribution on the molecule in Figure 5 is symmetrical, and the level of polarity is low.

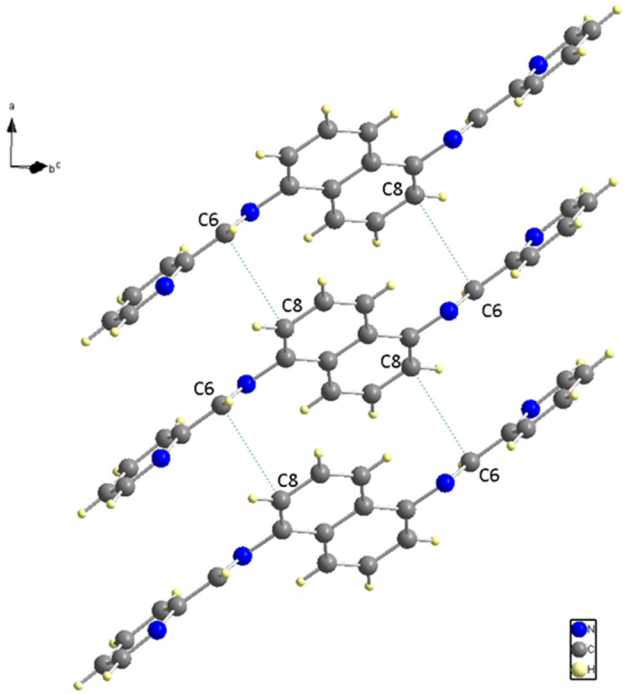

Figure 4. Neighboring Molecules Short contacts.

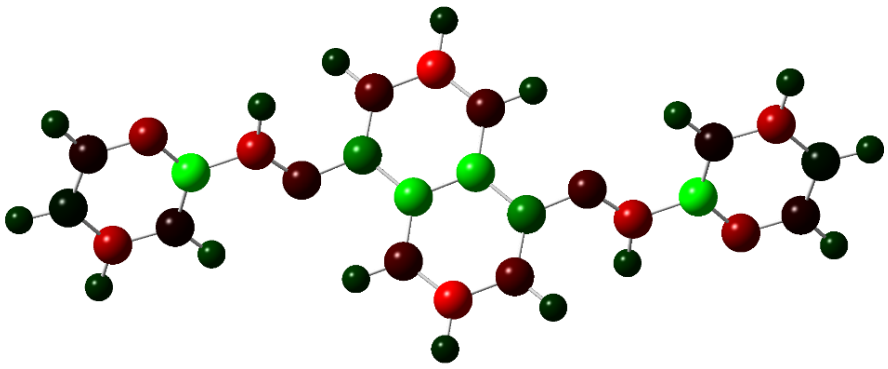

Figure 5. Charge distribution with a color range from −0.614 to 0.614 Mulliken (red for negative, green for positive).

Figure 6 displays the structures of HOMO and LUMO, with E_{HOMO} and E_{LUMO} values of 0.20847 (eV) and 0.08374 (eV), respectively. To investigate noncovalent interactions in the solid state, we utilized Hirshfeld Surfaces analysis on the ligand. Figure 7 displays all the Hirshfeld properties. When the contact distance between atoms inside and outside the surface is greater than the sum of their respective van der Waals radii, the areas in blue on the d_{norm} property are indicated. The d_{norm} property has white areas that correspond to a contact distance equal to the sum of the van der Waals radii, and small amounts of red areas where the contact distance between atoms inside and outside the surface is less than the sum of their respective van der Waals radii [29].

The red areas on the plot represent non-covalent regions, and they are primarily located on the C6 and C8 atoms, which we identified in Figure 4 as being associated with these interactions. Figure 8 displays the fingerprint plot, which provides a visual representation of the interactions involved and their respective percentage contributions to the total interactions.

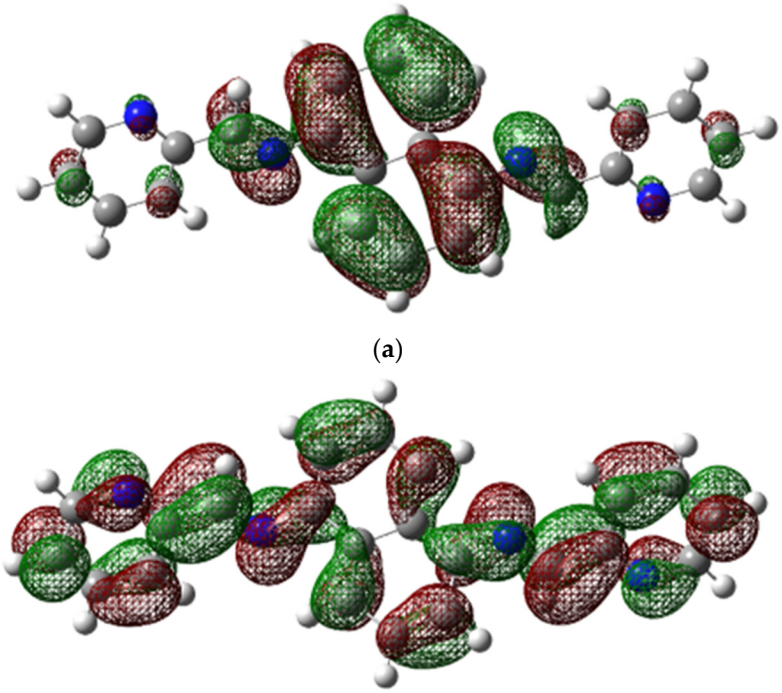

(**a**)

(**b**)

Figure 6. (**a**) HOMO and (**b**) LUMO structures.

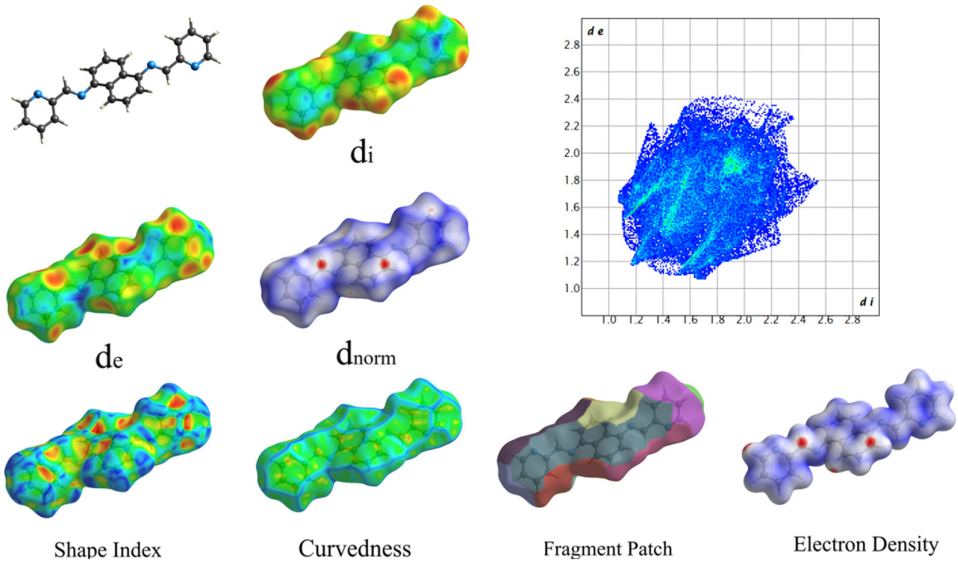

Figure 7. Hershfield Surfaces mapper with all properties (a: −0.97, b: 0.08, c: 0.21).

According to Figure 8, the primary interaction throughout the surface is dispersion forces (H···H), which account for over 45% of the total interactions. The combined percentage of H and C in the structure is 29.2%, which includes contributions from both H(i)···C(e) and C(i)···H(e) interactions. Additionally, the total contribution of N and H is 14.6%. Therefore, carbon and hydrogen, with a contribution of 29.2%, along with the C8 and C6 interaction and dispersion forces (H···H), as depicted in Figure 9, are the forces that govern the stacking arrangement of the ligand molecules.

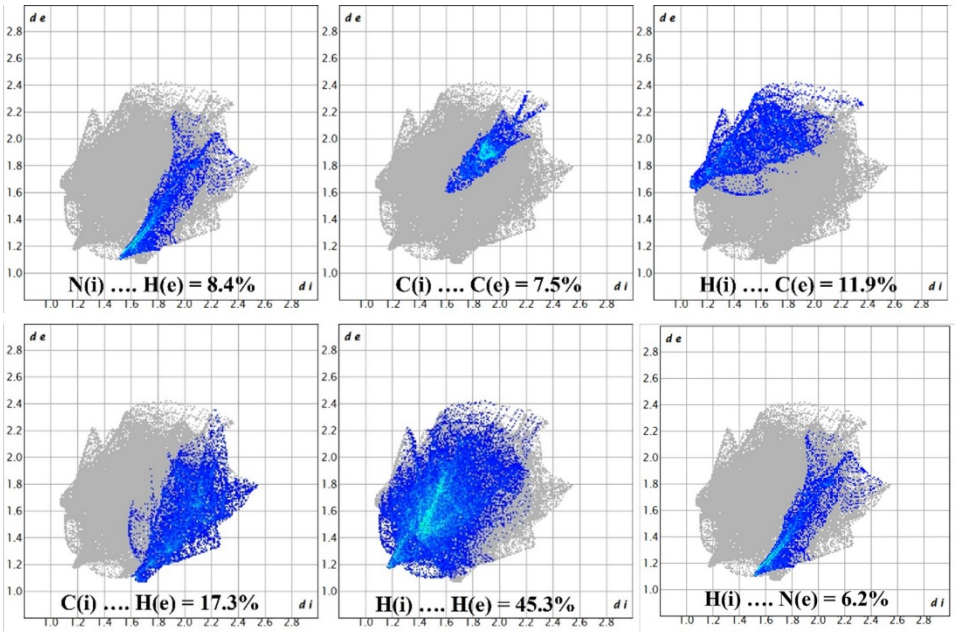

Figure 8. Demonstration of percentage contributions in the total interactions.

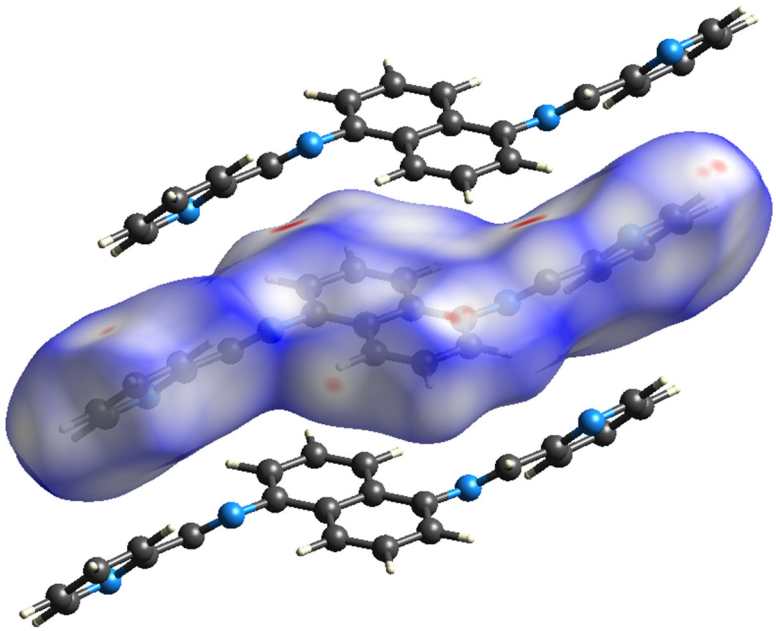

Figure 9. Hirshfeld surface.

The ligand being discussed can potentially form coordination complexes with multiple metals. Some of the metals that have been utilized to create coordination complexes with Schiff base ligands, which have structural similarities to our synthesized ligand, are Co (II), Ni (II), Cu (II), Zn (II), gold (III), and copper (II) [30–33]. Furthermore, the ligand has the potential to create coordination complexes with other transition metals, including Pd (II) [34]. The coordination geometry of metal complexes may differ based on the specific metal involved, although octahedral coordination is preferred for certain metals [30]. The crystal structures of metal complexes may differ based on the metal used and the coordination geometry formed. As an example, in a previous study [31], the author reported on gold (III) complexes with 1,1-dimethylbiguanide. In this case, the gold atom is coordinated by two chloride ligands and two nitrogen atoms from the biguanide ligand, resulting in a square planar coordination geometry.

4. Conclusions

In conclusion, we successfully synthesized and characterized a symmetrical ligand, N, N′-(naphthalene-1,5-diyl) bis(1-(pyridin-2-yl) methanimine), through refluxing 1,6-diaminonaphthalene and pyridine-2-carbaldehyde in extra-pure ethanol. The ligand was found to have a structure containing central naphthalene and two parallel parts on the sides, with two pyridylimine-binding units connected to a 1,5-naphthalene structure. The structure was confirmed through infrared examination, and computational spectroscopy and theoretical methods were used to show the ligand HOMO, LUMO, and charge distribution. Additionally, we conducted a Hirshfeld analysis and demonstrated all of its properties. Our findings suggest that dispersion forces (H···H) were the primary factor contributing to the arrangement of the ligand molecule, accounting for 45.3% of the total interactions in the absence of hydrogen bonding.

Supplementary Materials: Crystallographic data for the structure reported in this paper have been deposited with the Cambridge Crystallographic Data Centre as supplementary publication CCDC-2252233 for $C_{22}H_{16}N_4$ (**1**). Copies of the data can be obtained by request from the CCDC, 12 Union Road, Cambridge CB2 1EZ, UK (Fax: +44-1223-336033, e-Mail: de-posit@ccdc.cam.ac.uk).

Author Contributions: B.M., writing—review and editing; A.K., validation, formal analyses, writing—original draft preparation and editing; N.R., writing—original draft preparation; Y.H., supervision, writing—review and editing and S.W.J., project administration and editing. All authors have read and agreed to the published version of the manuscript.

Funding: This work was funded by grant NRF-2019R1A5A8080290 of the National Research Foundation of Korea.

Data Availability Statement: Not applicable.

Acknowledgments: We thank the University of Qom for their assistance with this project.

Conflicts of Interest: The authors declare no conflict of interest.

References

1. Altintop, M.D.; Sever, B.; Özdemir, A.; Kuş, G.; Oztopcu-Vatan, P.; Kabadere, S.; Kaplancikli, Z.A. Synthesis and Evaluation of Naphthalene-Based Thiosemicarbazone Derivatives as New Anticancer Agents against LNCaP Prostate Cancer Cells. *J. Enzym. Inhib. Med. Chem.* **2016**, *31*, 410–416. [CrossRef] [PubMed]
2. Ibrahim, M.; Tashkandi, N.; Hadjichristidis, N.; Alkayal, N.S. Synthesis of Naphthalene-Based Polyaminal-Linked Porous Polymers for Highly Effective Uptake of CO_2 and Heavy Metals. *Polymers* **2022**, *14*, 1136. [CrossRef]
3. Meistermann, I.; Moreno, V.; Prieto, M.J.; Moldrheim, E.; Sletten, E.; Khalid, S.; Rodger, P.M.; Peberdy, J.C.; Isaac, C.J.; Rodger, A.; et al. Intramolecular DNA Coiling Mediated by Metallo-Supramolecular Cylinders: Differential Binding of P and M Helical Enantiomers. *Proc. Natl. Acad. Sci. USA* **2002**, *99*, 5069–5074. [CrossRef] [PubMed]
4. Lu, P.; Wang, Y.; Lin, J.; You, L. A Novel Synthesis Route to Rare Earth Polyborates. *Chem. Commun.* **2001**, *13*, 1178–1179. [CrossRef]
5. Janica, I.; Patroniak, V.; Samorì, P.; Ciesielski, A. Imine-Based Architectures at Surfaces and Interfaces: From Self-Assembly to Dynamic Covalent Chemistry in 2D. *Chem. Asian J.* **2018**, *13*, 465–481. [CrossRef]
6. Hamblin, J.; Childs, L.J.; Alcock, N.W.; Hannon, M.J. Directed One-Pot Syntheses of Enantiopure Dinuclear Silver(i) and Copper(i) Metallo-Supramolecular Double Helicates. *J. Chem. Soc. Dalton Trans.* **2002**, *2*, 164–169. [CrossRef]
7. Childs, L.J.; Alcock, N.W.; Hannon, M.J. Assembly of Nano-Scale Circular Supramolecular Arrays through π–π Aggregation of Arc-Shaped Helicate Units. *Angew. Chem. Int. Ed.* **2001**, *113*, 1079–1081. [CrossRef]
8. Hamblin, J.; Jackson, A.; Alcock, N.W.; Hannon, M.J. Triple Helicates and Planar Dimers Arising from Silver(i) Coordination to Directly Linked Bis-Pyridylimine Ligands. *J. Chem. Soc. Dalton Trans.* **2002**, *8*, 1635. [CrossRef]
9. Zaier, R.; Ayachi, S. Toward Designing New Cyclopentadithiophene-Naphthalene Derivatives Based Small Molecules for Organic Electronic Applications: A Theoretical Investigation. *Mater. Today Commun.* **2021**, *27*, 102370. [CrossRef]
10. Gondia, N.K.; Sharma, S.K. Comparative Optical Studies of Naphthalene Based Schiff Base Complexes for Colour Tunable Application. *Mater. Chem. Phys.* **2019**, *224*, 314–319. [CrossRef]
11. Li, Q.; Ma, L.; Li, J.; Wang, L.; Yu, L.; Zhao, Y.; Lv, Y. Study of a Fluorescent System Based on the Naphthalene Derivative Fluorescent Probe Bound to Al^{3+}. *Micromachines* **2023**, *14*, 868. [CrossRef] [PubMed]
12. Xu, X.; Cao, P.; Wang, Y.; Wu, W.; Guo, J.; Sun, J.; Zou, X.; Wang, W.; Ruan, H. Effects of Naphthalene Application on Soil Fungal Community Structure in a Poplar Plantation in Northern Jiangsu, China. *Appl. Sci.* **2023**, *13*, 5794. [CrossRef]

13. Sadek, O.; Bouhadir, G.; Bourissou, D. Lewis Pairing and Frustration of Group 13/15 Elements Geometrically Enforced by (Ace)Naphthalene, Biphenylene and (Thio)Xanthene Backbones. *Chem. Soc. Rev.* **2021**, *50*, 5777–5805. [CrossRef] [PubMed]
14. Nishino, M.; Miyashita, S. Effect of the Short-Range Interaction on Critical Phenomena in Elastic Interaction Systems. *Phys. Rev. B* **2013**, *88*, 014108. [CrossRef]
15. Melkikh, A.V.; Meijer, D.K.F. On a Generalized Levinthal's Paradox: The Role of Long- and Short Range Interactions in Complex Bio-Molecular Reactions, Including Protein and DNA Folding. *Prog. Biophys. Mol. Biol.* **2018**, *132*, 57–79. [CrossRef]
16. Claesson, P.M.; Kjellin, M.; Rojas, O.J.; Stubenrauch, C. Short-Range Interactions between Non-Ionic Surfactant Layers. *Phys. Chem. Chem. Phys.* **2006**, *8*, 5501. [CrossRef] [PubMed]
17. Kotelchuck, D.; Scheraga, H.A. The Influence of Short-Range Interactions on Protein Conformation, ii. a Model for Predicting the α-Helical Regions of Proteins. *Proc. Natl. Acad. Sci. USA* **1969**, *62*, 14–21. [CrossRef]
18. Den Besten, G.; van Eunen, K.; Groen, A.K.; Venema, K.; Reijngoud, D.-J.; Bakker, B.M. The Role of Short-Chain Fatty Acids in the Interplay between Diet, Gut Microbiota, and Host Energy Metabolism. *J. Lipid Res.* **2013**, *54*, 2325–2340. [CrossRef]
19. Youinou, M.-T.; Rahmouni, N.; Fischer, J.; Osborn, J.A. Self-Assembly of a Cu_4 Complex with Coplanar Copper(I) Ions: Synthesis, Structure, and Electrochemical Properties. *Angew. Chem. Int. Ed. Engl.* **1992**, *31*, 733–735. [CrossRef]
20. Baxter, P.N.W.; Lehn, J.-M.; Fischer, J.; Youinou, M.-T. Self-Assembly and Structure of a 3 $\times$ 3 Inorganic Grid from Nine Silver Ions and Six Ligand Components. *Angew. Chem. Int. Ed. Engl.* **1994**, *33*, 2284–2287. [CrossRef]
21. Piontek, A.; Siodłak, D.; Zarychta, B. Naphthalene-2,6-Diyl Bis(4-Methylbenzenesulfonate). *IUCrdata* **2018**, *3*, x180890. [CrossRef]
22. Bruker. *SADABS, Version 2008/1*; Bruker AXS Inc.: Madison, WI, USA, 2008.
23. Bruker. *XPREP, Version 2008/2*; Bruker AXS Inc.: Madison, WI, USA, 2008.
24. Bruker. *SAINT, Version 7.68A.*; Bruker AXS Inc.: Madison, WI, USA, 2009.
25. Bruker. *APEX2, Version 2010.3-0*; Bruker AXS Inc.: Madison, WI, USA, 2010.
26. Sheldrick, G.M. A Short History of *SHELX*. *Acta Crystallogr. A* **2008**, *64*, 112–122. [CrossRef] [PubMed]
27. Cromer, D.T.; Waber, J.T. *International Tables for X-ray Crystallography*; Kynoch Press: Birmingham, UK, 1974; Volume 4, Table 2.2 A.
28. Spackman, P.R.; Turner, M.J.; McKinnon, J.J.; Wolff, S.K.; Grimwood, D.J.; Jayatilaka, D.; Spackman, M.A. *CrystalExplorer*: A Program for Hirshfeld Surface Analysis, Visualization and Quantitative Analysis of Molecular Crystals. *J. Appl. Crystallogr.* **2021**, *54*, 1006–1011. [CrossRef] [PubMed]
29. McKinnon, J.J.; Jayatilaka, D.; Spackman, M.A. Towards Quantitative Analysis of Intermolecular Interactions with Hirshfeld Surfaces. *Chem. Commun.* **2007**, *7*, 3814. [CrossRef] [PubMed]
30. Abouelatta, A.I.; Sonk, J.A.; Hammoud, M.M.; Zurcher, D.M.; McKamie, J.J.; Schlegel, H.B.; Kodanko, J.J. Synthesis, Characterization, and Theoretical Studies of Metal Complexes Derived the Chiral Tripyridyldiamine Ligand Bn-CDPy3. *Inorg. Chem.* **2010**, *49*, 5202–5211. [CrossRef]
31. Makotchenko, E.V.; Kharlamova, V.Y.; Baidina, I.A.; Bardina, E.E.; Korolkov, I.V.; Mironov, I.V.; Gushchin, A.L. Synthesis, Crystal Structure and Solution Studies of Gold(III) Complexes with 1,1-Dimethylbiguanide. *Inorganica Chim. Acta* **2023**, *552*, 121496. [CrossRef]
32. Murillo, J.; Goodwin, C.A.P.; Stevens, L.; Fortier, S.; Gaunt, A.J.; Scott, B.L. Synthesis and Comparison of Iso-Structural f-Block Metal Complexes (Ce, U, Np, Pu) Featuring η^6-Arene Interactions. *Chem. Sci.* **2023**, *14*, 7438–7446. [CrossRef]
33. Kollur, S.P.; Castro, J.O.; Frau, J.; Flores-Holguʻın, N.; Shruthi, G.; Shivamallu, C.; Glossman-Mitnik, D. Preparation, Spectroscopic Investigations and Chemical Reactivity Properties of a New Schiff Base Ligand and Its Copper (II) Complexes. *J. Mol. Struct.* **2019**, *1191*, 17–23. [CrossRef]
34. Kurpik, G.; Walczak, A.; Gołdyn, M.; Harrowfield, J.; Stefankiewicz, A.R. Pd(II) Complexes with Pyridine Ligands: Substituent Effects on the NMR Data, Crystal Structures, and Catalytic Activity. *Inorg. Chem.* **2022**, *61*, 14019–14029. [CrossRef]